FINAL REPORT

NASA Cooperative Agreement Number NCC25003

The Velocity and Vorticity Fields of the Turbulent Near Wake of a Circular Cylinder

Principle Investigator: James Wallace

Co-Investigator: Lawrence Ong

NASA-Ames Collaborator: Parviz Moin

Department of Mechanical Engineering
University of Maryland
College Park, MD 20742

January 1995

The Velocity and Vorticity Fields of the Turbulent Near Wake of a Circular Cylinder.

Lawrence Ong & James Wallace
Department of Mechanical Engineering
University of Maryland
College Park, MD 20742

1 Introduction

This project is a Joint Research Interchange between the NASA Ames Research Center/Center for Turbulence Research(CTR) and the University of Maryland/Turbulence Research Laboratory(TRL), NASA Cooperative Agreement Number NCC25003. The purpose of this research is to provide a detailed experimental database of velocity and vorticity statistics in the very near wake ($x/d < 10$) of a circular cylinder at Reynolds number of 3900.

1.1 Present accomplishments

Velocity measurements in this flowfield are extremely difficult due to the high velocity vector angles of attack and relative low flow velocity magnitudes, especially at locations very near the cylinder and along centerline of its wake. Preliminary exploratory measurements with a single sensor probe yielded unphysically high fluctuations in measured streamwise velocity component (u). This result led to a detailed analysis to determine the accuracy of single and X-wire probes in flows with high angles of attack. Following the analysis, the use of a single wire probe for the present study was abandoned in favor of X-wires probe measurements. A brief comparison between two methods for reducing X-wire data, the Cosine-law and the Look-Up Table(LUT) techniques, was also performed.

A set of wake velocity profiles have been obtained at the several axial stations downstream of the circular cylinder: $x/d = 3, 4, 5, 6, 7$ & 10. Statistical properties of the streamwise(u) and normal(v) velocity components of velocity, the u and v spectra, and an estimate of the spanwise correlation length are presented later in this report.

Additionally, simultaneous measurements all three velocity components were made with a 4-wire probe along the wake centerline. The 4-wire probe used here has an approximate sensing area of $1mm \times 1mm$, which is about twice as large than the X-wire probe used for the detailed measurements. This set of measurements was conducted to explore the extent of the three-dimensionality of the wake and thus provide a semi-quantitative test of the X-wire measurements which, of necessity, assume a 2-D flowfield. Spanwise spatial

Coordinate axis	Velocity component[†]	Nomenclature Used
x	u	Streamwise, axial
y	v	vertical, normal (to the cylinder's axis)
z	w	spanwise, parallel (to the cylinder's axis)

Table 1: Coordinate axis and associated velocity components.

correlation measurements were also performed with a rake of single sensor probes.

2 Experimental apparatus and procedure

The experiments were conducted at the windtunnel at the Turbulence Research Laboratory, University of Maryland. The test-section of the windtunnel has a rectangular exit cross-section of $1.2(width) \times$ and $0.7m$(height) . For the present experiments, a circular cylinder, with a diameter of $14.3cm$ was mounted at approximately $7.3m$ from the end of the contraction, and at the tunnel's half-height location. The cylinder's longitudinal axis was aligned in the spanwise (z) direction of the windtunnel A 3-axis traversing device enables motor-driven probe positioning in the y and z directions and manual probe positioning in the x-direction. The same coordinate system, listed in Table 1, is used for both the flow facility and the probe (See also Figs. 5).

The hot-wire probes were operated in the constant temperature mode with an A.A. Lab Systems Hot-wire Anemometer System at overheat ratios of 1.2 and 1.35, for the 4-wire and X-wire probes respectively. The tunnel velocity was monitored using a pitot-static probe connected to a Barocel Electronic Manometer with range of 0-1 Torr and a resolution of 10^{-5} torr. The uncertainty in absolute velocity value is approximately $\pm 0.05m/s$ (or about $\pm 1\%$ of the present freestream velocity of $4.2m/s$).

The outputs of the above transducers were digitized by a Optim Megadac 5018 16-bit Data Acquisition System which has a maximum data throughput of 250kHz. This system was controlled by a personal computer via an IEEE 488 interface. The digitized data were immediately streamed to the PC's hard disk for temporary storage. The acquired data sets were transmitted to a Sun Microsystem's workstation for further data analysis and archival storage on tape.

A compact compressed-air driven jet was used to calibrate the hot-wire probes. This jet, with a circular exit nozzle diameter of $30mm$ and a contraction ratio of 2.56, is mounted on a motorized angular displacement mechanism, enabling automated probe

---

[†]Herein, uppercase variables denote instantaneous values, lowercase variables denote fluctuations about average values, overbars denote time averaged values, and superscript primes denote *rms* values.

calibration for pitch and/or yaw responses. The jet's pitch and yaw axis is centered along it's longitudinal axis and located approximately $5mm$ from the jet exit plane. Probes to be calibrated are placed approximately at this center of rotation, which is well within the jet's potential core region. The pressure drop across the nozzle itself had been pre-calibrated against the flow speed (measured with a pitot-static tube), and is used to monitor the jet's exit flow speed.

A summary of the experimental parameters is listed below:

- Freestream Velocity, $U_\infty \approx 4.2 \; m/s$
- Reynolds Number based on cylinder diameter, $Re_d \approx 3900$,
- Freestream Turbulence intensity $\approx 0.67\%$
- Data Acquisition digitization rate $= 6912 Hz$.
- Pre-digitization analog low-pass filter cutoff frequency $= 2564 Hz$.

2.1 Hot-wire probes

The miniature combination probe consisting of 2 normal hot-wires and an X-wire pair was used in the present measurements. While the signals from all the 4 hot-wire sensors were acquired and digitized, only the X-wire data were used for the present study. The X-wires have sensors of approximately $0.6mm$ length. The sensors are spaced $0.4mm$ from each other and are oriented at an angles of approximately $\pm 40^o$, from the horizontal axis. For reasons to be described in the following sub-section, the Look-Up-Table (LUT) technique of Gresko[8] was used to reduce the definitive X-wire data presented in this report. A brief analysis of the effects due to bi-normal cooling on X-wire data is also given later.

The measurements to obtain estimates of the spanwise correlation length were obtained with a rake consisting of 20 normal hot-wires. Only 12 of the 20 hot-wire sensors in this rake were used in the present measurements. The positions of the sensors (each nominally $2mm$ in length) are shown in Table 2. The rake was operated in the constant temperature

Sensor Number, i	1	2	3	4	5	7	9	10	12	14	16	18
Distance form Sensor 1, $z \, [mm]$	0	1.91	3.9	5.8	7.9	11.8	15.7	17.5	21.4	25.4	29.3	33.1
Sensor separation, $z/d = (z_0 - z_i)/d$	0	0.13	0.27	0.41	0.55	0.83	1.10	1.23	1.50	1.78	2.05	2.32

Table 2: Rake Dimensions.

mode with an overheat of 1.4. The hot-wire voltages were not linearized since the cross correlation coefficients reflect only the phase differences between the sensors. The sensors of this probe were oriented in a plane normal to the axis of the cylinder.

3

3 Experimental evaluation of errors due to bi-normal cooling

There have been numerous attempts to account for the effects of binormal cooling on hot-wire measurements [6, 13]. In order to measure the turbulence intensities and/or the Reynolds stresses, these methods often involve:

- multi-orientation of the probes,

- decomposition of the hot-wire response equations into the mean and fluctuating parts, and

- the neglection of higher order terms or correlations.

Therefore, of necessity, these methods are restricted to use in flows with low turbulence intensities ($< 10\%$). It should be noted that prior knowledge of the direction of the mean flow vector is not always available in a fully 3-D flowfield.

3.1 Single-sensor (normal) hot-wire probe results

In this evaluation, the calibrated (at zero pitch and yaw angles) single-sensor probe was placed in the potential core flow of calibration jet, which was re-oriented at a variety of pitch and yaw angles relative to the probe's horizontal axis. Figure 1 shows the error incurred at various pitch and yaw angles when it is assumed that $u \approx U_{eff}$, where U_{eff} is the effective cooling velocity as defined by Bradshaw[2]. This plot shows that for pitch angles of $< 5^o$, the estimate of streamwise velocity component u is within 5%. At higher pitch angles, the error incurred with this assumption is much greater, e.g. $+25\%$ at pitch angle $= 30^o$. Three-dimensionality (non-zero yaw) adds to the inaccuracy. As expected, u is always overestimated at all non-zero pitch angles as the U_{eff} physically reflects the induced flow magnitude as discussed next.

The plot in Fig. 2 represents the difference between the magnitude of the induced velocity and U_{eff} obtained by the calibrated single sensor probe when it is misaligned with the induced flow velocity vector. Such misalignment is unavoidable when a probe is placed in an unknown two or three dimensional flowfield. Increasing the pitch angle resulted in an increase of the percent error due to binormal cooling effects. Compared to the larger error in recovering the u-component, where error are $> 25\%$ at the extreme pitch angles, the error curves in this plot are contained within the $\pm 10\%$ band throughout pitch and yaw angle ranges examined here. This result indicates that single sensor probes performs quite adequately (within $\pm 10\%$ for pitch and yaw angles $< \pm 25^o$) as a velocity magnitude measurement device. This plot also shows the expected decrease in cooling efficiency with increasing yaw angle, e.g. at pitch angle $= 0^o$ the error is negative for yaw angles $> 0^o$.
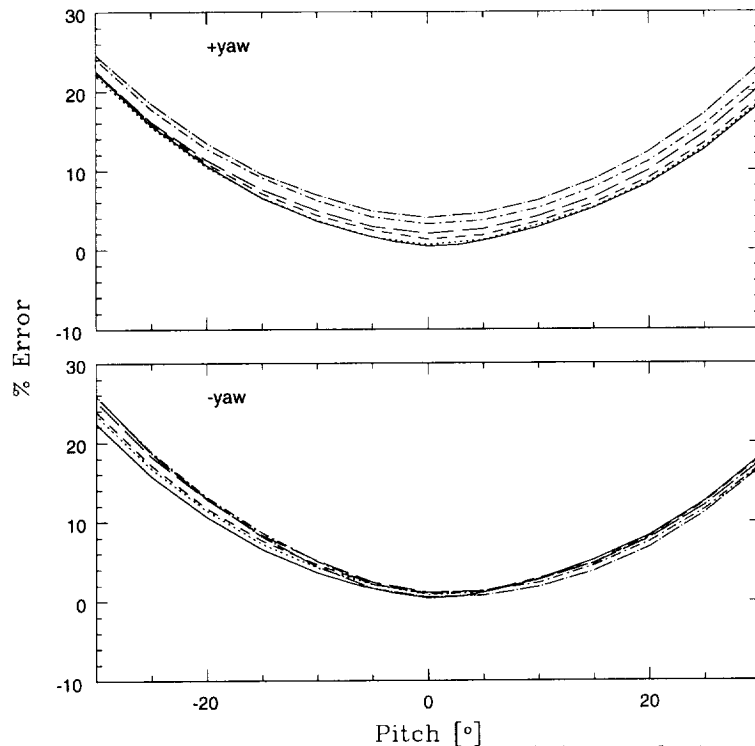
4

Figure 1: Error in single hot-wire measurements of the u-velocity component at selected yaw angles[°]: —— 0, ········ 5, --- 10, ———— 15, —·— 20, ——— 25.
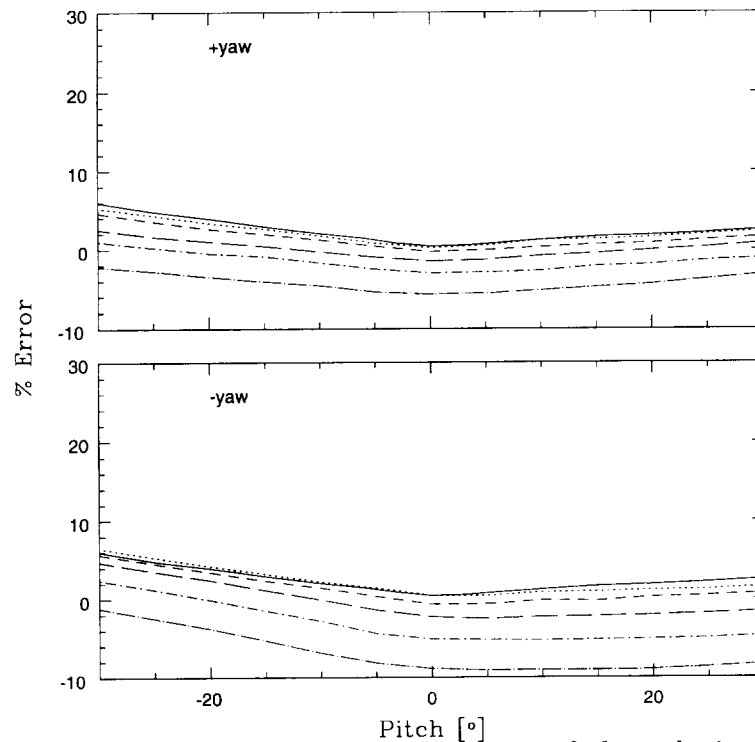

Figure 2: Error in single hot-wire measurements of the velocity vector magnitude at selected yaw angles (Symbols are described in Fig. 1).
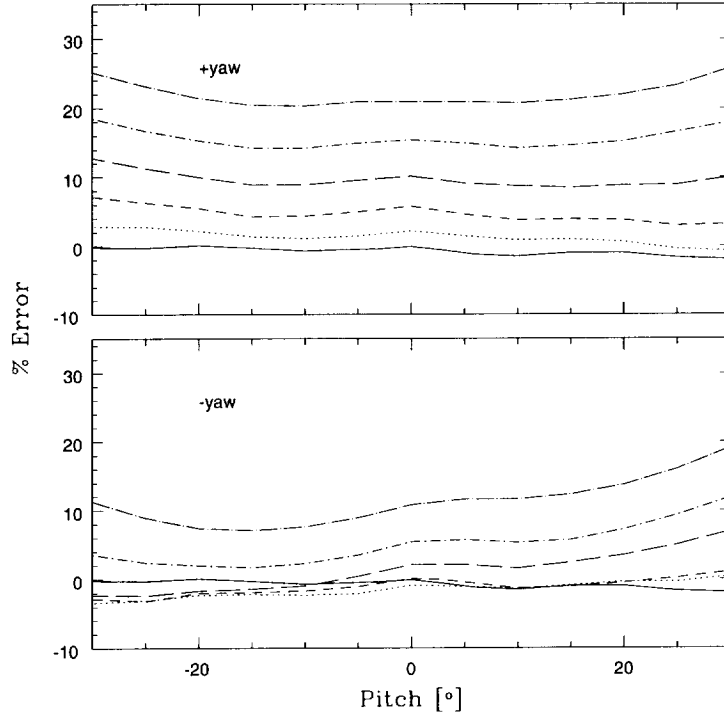
Figure 3: Error in X-wire measured u-velocity component due to binormal cooling at selected yaw angles (Symbols are described in Fig. 1).

3.2 X-wire probe results

This evaluation of the effects of bi-normal cooling on X-wire probes was performed by first calibrating the X-wire in the manner described previously. As in the test with the single-wire probe, the response of the X-wire probe was then determined for a variety of pitch and yaw angles.

Figures 3 and 4 shows the error between the induced velocity components and the data recovered from the X-wire using the LUT technique. The presence of the binormal cooling causes an overestimation of the recovered u-velocity component for both positive and negative yaw orientations. This result is expected because the binormal cooling components tend to experience less blockage from the prongs, resulting in more efficient cooling of the sensors. The errors for the present probe was found to be as much as 30% of the induced streamwise velocity component at 30° yaw. The small negative error in the negative pitch and yaw region can be attributed to slight misalignment of the probe in the vertical plane. The magnitude of measured v velocity component is also over estimated when yaw angle $\neq 0$ as shown in Fig. 4.

Therefore, the use of X-wires for instantaneous velocity measurements in 3-D flows where the angle of attacks exceed 10° can result in errors of up to 30% for the u velocity
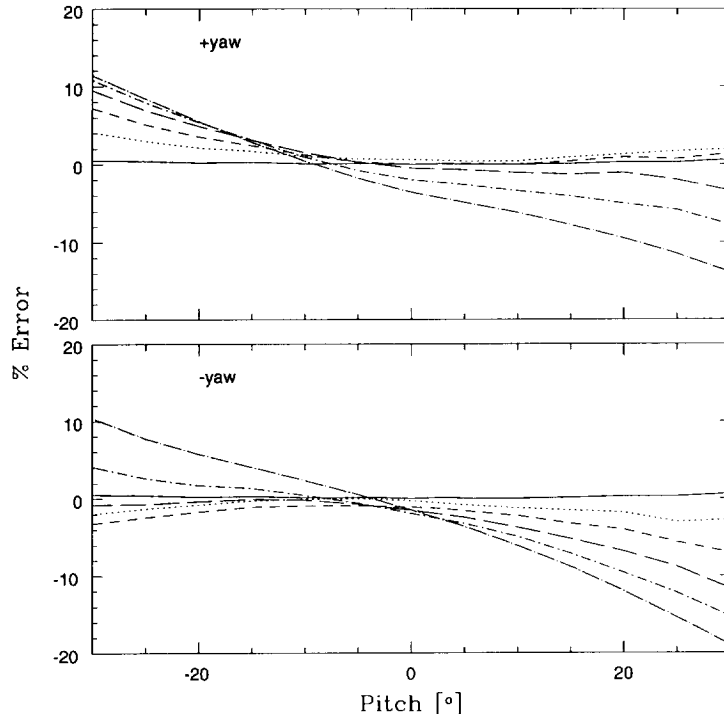
6

Figure 4: Error in X-wire measured v velocity component due to binormal cooling at various yaw angles (Symbols are described in Fig. 1).

component and 20% for the v velocity component. The cosine law results (not shown here) gave less accurate data recovery and does not have a flat error response, tending to give larger overestimates at the extreme yaw angles.

4 Comparison X-wire data reduction techniques

There are basically two methods used to reduce X-wire data. The first, classically known as the cosine law method, attempts to obtain a general empirical description of the cooling of a hot-wire as a function of flow angles. This method had been extensively studied by various researchers and is very well documented in the literature (e.g. Bradshaw[2], Brunn[4] and, Friehe and Schwarz[7]). Using first order approximations and with multiple orientation of the X-probe, previous researchers were able to approximate the time-averaged, but not the instantaneous, Reynolds shear and normal stresses[5, 13]. The use of these multi orientation methods are also limited to flows with low turbulence intensities ($< 10\%$).

The second method which is the LUT technique first introduced by Willmarth & Bogar[15], simply maps each calibration voltage pair to the two induced velocity compo-

7

nents u and v. Other techniques utilizing look-up-table methods include those of Johnson and Eckelmann[9] and Lueptow et al.[11]. Gresko[8] further refined the technique of Lueptow et al.[11] by remapping the calibration map in polar cordinates. Gresko's implementation of the LUT method has been used for the present X-wire data reduction and is described briefly later in this report.

In their recent study, Browne[3] and his co-workers concluded that in the measurement of instantaneous flow quantities in strictly 2-D flows, both methods yield similar results in flows with low mean angles of attack ($< \pm 15^o$) even when the turbulence intensities were high. They also found significant deviations of the cosine law at high angle of attacks (concurring with the findings Friehe and Schwarz[7] and others), and recommended that the LUT method with extended calibration ranges be used for such flows. However, the effects of bi-normal cooling, inherently present in 3-D flow fields was not addressed in their investigation.

4.1 Cosine-law data reduction procedure

The effective cooling velocity sensed by the probe can be described by a 4th order polynomial fit of the anemometer's output voltage(E):

$$P(E) = U_{eff}^2 = A_1 + A_2 E + A_3 E^2 + A_4 E^3 + A_5 E^4, \tag{1}$$

In general, cosine-law methods further decomposes U_{eff} into the various components of velocity. In the present implementation, following Jorgensen[10], for each wire of the X-probe:

$$U_{eff}^2 = u_n^2 + k_1^2 u_t^2 + k_2^2 u_{bn}^2, \tag{2}$$

where u_n, u_t and u_{bn} are the velocity components with respect to the sensor coordinate system as shown in Fig. 5.

The coefficients k_1 and k_2 are the pitch and yaw factors, as defined by Jorgensen[10], which weight the cooling due to the components u_t and u_{bn}. One can also relate these velocity components to the components in the flowfields' coordinate system by geometrical considerations.

$$u_n = u cos\alpha + v sin\alpha,$$
$$u_t = u sin\alpha + v cos\alpha,$$
$$u_{bn} = w, \tag{3}$$

where α is the angle made by the sensor with the flow's x-axis. More generally,

$$u_n = n_1 u + n_2 v + n_3 w,$$
$$u_t = t_1 u + t_2 v + t_3 w, and$$
$$u_b n = b_1 u + b_1 v + b_1 w, \tag{4}$$

8

y

Inclined
sensor in the
x-y plane
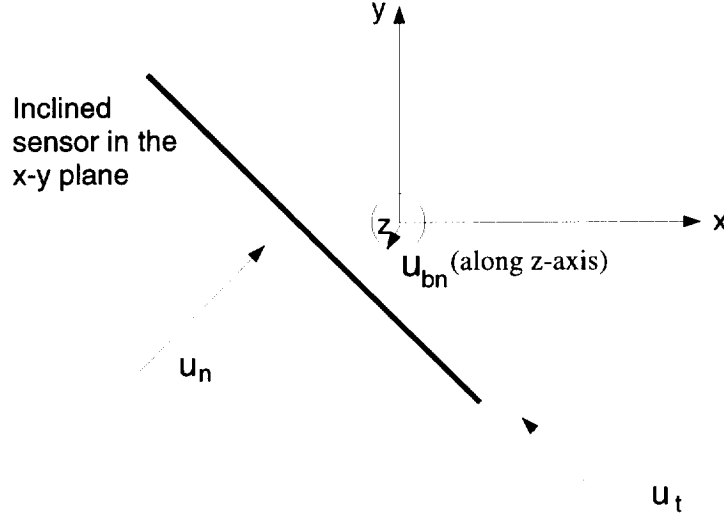
z

U_{bn} (along z-axis)

x

U_n

U_t

Figure 5: Probe coordinate system.

where n_i, t_i and b_i are the flowfield-sensor coordinate transformation coefficients. However, accurate measurements of the required angles for miniature probes are difficult. Additionally, due to physical effects such as bowed wires, flow blockage due to the prongs, the effective angle (see Bradshaw[2]) is not equal to the physical angle. As this effective angle can only be obtained from calibration, it is more convenient to directly calibrate for the combined geometrical-physical coefficients via a modified cooling law from the above equations (eg. Marasli et al.[12]):

$$U_{eff}^2 = u^2 + C_1 v^2 + C_2 w2 + C_3 uv + C_4 uw + C_5 vw, \tag{5}$$

obtained by substituting Eqns.(4) into Eqn.(2) and giving new symbols $C_i(i = 1 - 5)$ to the coefficients.

For the X-wire probes, the terms involving one of the cross-stream components must be eliminated from the above equation so that a determinate coupled set of equations can be formed. In this study, for measurement of the u and v velocity fluctuations, the probe is oriented with the wires in the $x - y$ plane . Therefore terms involving w were removed, and when combined with Eqn.(1) the response equation for each sensor (i) is:

$$P(E)_i = u^2 + C_{1i} v^2 + C_{3i} uv, \tag{6}$$

which can then be solved simultaneously.

4.2 Look-up-table data reduction procedure

As in all calibrations involving the use of X-wires, the LUT calibration procedure involves recording the voltage outputs of the hot-wire anemometers at various angles. However,
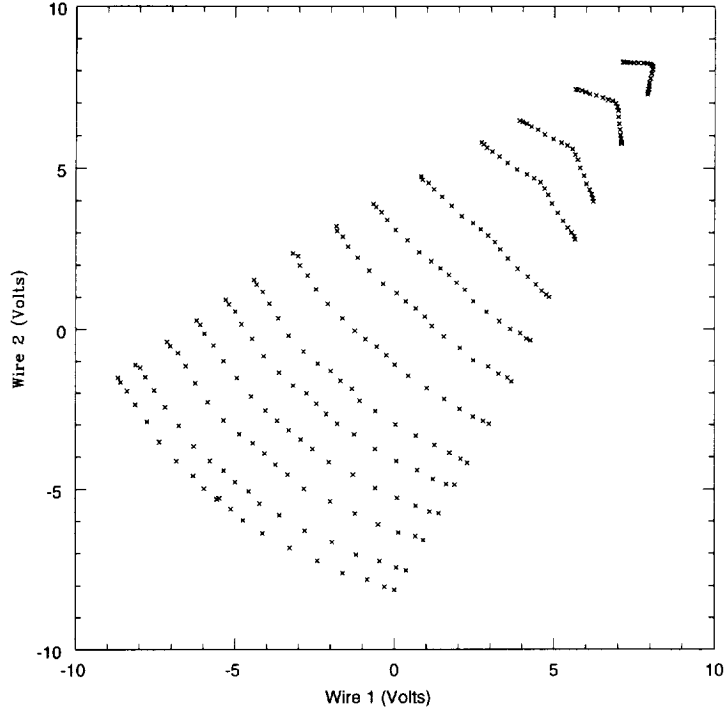
9

Figure 6: Typical calibration voltage pairs.

here is where the similarity ends. The LUT method, basically an interpolation procedure, requires a much finer calibration grid (i.e. more calibration data points) in order to have sufficient resolution. However, as the following results show, the operating angle of attack range is much more extended than that of the cosine law method.

Gresko's[8] LUT implementation, used in the present study, remaps the voltage pair for each calibration angle in polar coordinates. Figure 6 shows the fan-like plot of the hot-wire voltages (E_1 and E_2) of a typical calibration set. Here, the rationale behind the polar remapping is easily seen. Points along each 'arc' represents different pitch angles for a calibration subset at one speed. Calibration subsets with the higher flow speeds lie on 'arcs' with the larger radii. The polar calibration grid is constructed by first converting the hot-wire voltage pairs into polar coordinates by:

$$r = \sqrt{(E_1 - E_{1_{origin}})^2 + (E_2 - E_{2_{origin}})^2} \tag{7}$$

$$\beta = tan^{-1}[\frac{E_2 - E_{2_{origin}}}{E_1 - E_{1_{origin}}}] \tag{8}$$

where $E_{1_{origin}}$ and $E_{2_{origin}}$ is where the intersection of the outer radial lines (i.e. the angular limits of the calibration). Cubic splines are fitted along each calibration angle θ for both the flowrate(Q) and the angular polar coordinate β as functions of r. Then at regular intervals of r, β and Q at constant θ are evaluated. Similary, using cubic splines fitted for the Q and θ values for any given r as functions of β, Q and θ are determined for every grid node. Pairs of voltages from a calibrated probe can then be mapped onto this grid. Linear interpolation is used for points falling between nodes.

10

4.3 Comparison of the Cosine-law vs. LUT technique

Comparisons of the data recovery accuracy between the cosine law and the LUT reduction techniques are plotted in Fig. 7 and 8, for the u and v velocity components respectively. The plots, for several calibration velocities ranging from 0.5 to 6 m/s, shows the error between the measured and the induced velocity as a percentage of the induced velocity magnitude. The LUT method shows better accuracy in data recovery for both velocity components (note the change in scale on the plots). The cosine-law method did not converge for calibration velocities below $1m/s$. In this experiment, the calibration coeffents for the cosine law were obtained from all the available data (i.e a global fit). At the expense of additional programming complexities, the performance for the cosine-law would probably improve if regional calibration coefficients sets (each for limited flow velocities and pitch angle range) had been used instead. With multiple sets of calibration coefficients, transitions at the borders of each calibration range must be carefully handled to avoid data discountinuites. Further work is recommended for a more detailed comparison between the two data reduction schemes.

These comparison plots also show that, especially for the v velocity component, the errors increase with increasing pitch angle. On the other hand, for calibration velocites of $1m/s$ and higher, the small LUT error ($\pm 1\%$) is fairly flat across the range of pitch angles shown here. This finding concurs with that of Browne et al.[3]. While they had reported that the cosine law is not accurate for angles above 15° compared to the LUT method, data from the present probe shows that the response of the cosine law is quite flat for velocities greater than $2m/s$ when the pitch angles are $\pm 25^o$.

5 4-wire data reduction technique

A schematic of the 4-wire hot-wire probe is shown in Figure 9. The response equations for each of the 4-hot-wires can be written as,

$$P_i(E) = u^2 + C_1 v^2 + C_2 w2 + C_3 uv + C_4 uw + C_5 vw. \qquad (9)$$

The present data reduction scheme treats the probe as a pair of V-shaped probes - a vertical pair (consisting of wires 1 and 3) and horizontal pair (consisting of wires 2 and 4). The iterative Newton's scheme, begins by solving for the u and v velocity components using the response equations from the vertical wire pair and with w initially set to zero. The resultant u and v velocity components from the first step is then used in the response equations for the horizontal wire pair to obtain u and w. With each iterative step the lastest values for u , and v or w, is used and the process is repeated until the velocity components converge.
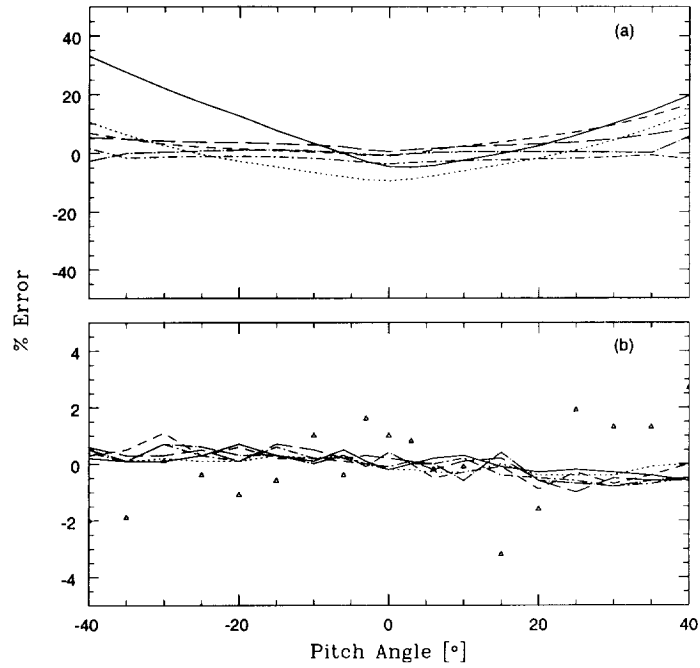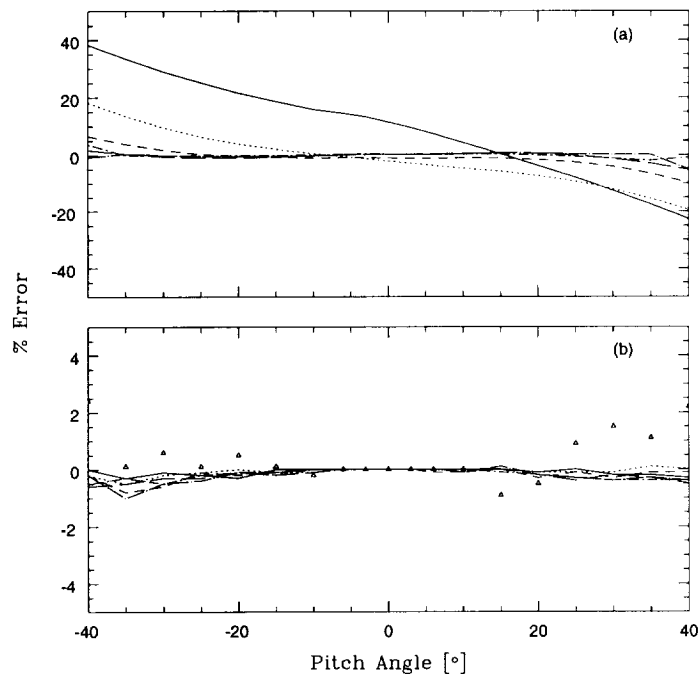
Figure 7: Error in recovering induced u velocity component from (a)Cosine Law method, (b) LUT method, at selected calibration flow speeds, V_c [m/s]: △ 0.5, —— 1, ········ 2, - - - 3, — — — 4, —·— 5, —·— 6.

Figure 8: Error in recovering induced v velocity component from (a)Cosine Law method, (b) LUT method, at selected calibration flow speeds, V_c. (Symbols are described in Fig. 7).
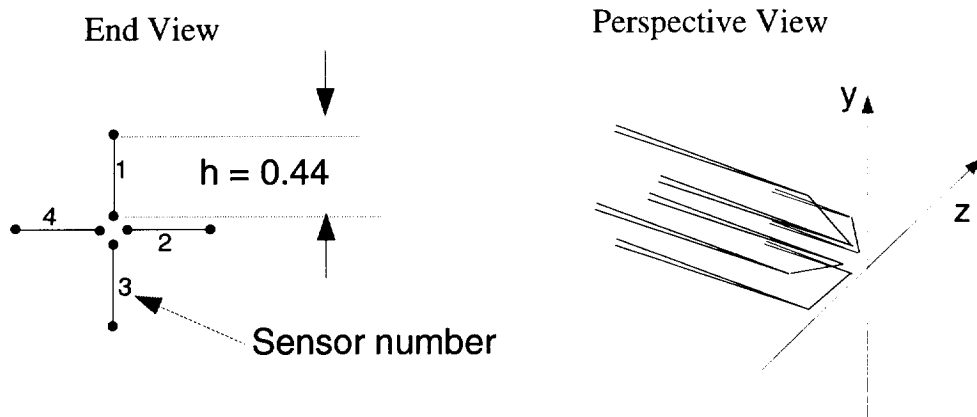
12

Figure 9: Schematic of the 4-sensor hot-wire probe.

6 Cylinder Wake Measurements

The measured vortex shedding frequency is approximately $64Hz$ corresponding to a Strouhal Number, $St \approx 0.21$. With a sampling duration of nearly $120s$ at $6912Hz$, each measurement recorded the velocity signatures of approximately 7680 vortex cycles. Although, only half (or $60s$) of data were necessary to achieve stable mean statistical results for each measurement, all $120s$ of each data set were used to ensure full convergence.

6.1 Mean Statistics

The mean, rms, skewness and flatness profiles of the u and v velocity components are plotted on Figs. 10 and 11, respectively. The Reynolds shear stress (uv) profiles at various x/d locations are plotted in Fig. 12. Also plotted on these figures, where available, are the LES results of Beaudan and Moin[1], and those of Zhou and Antonia[16]. The symbols used are given in Table 3:

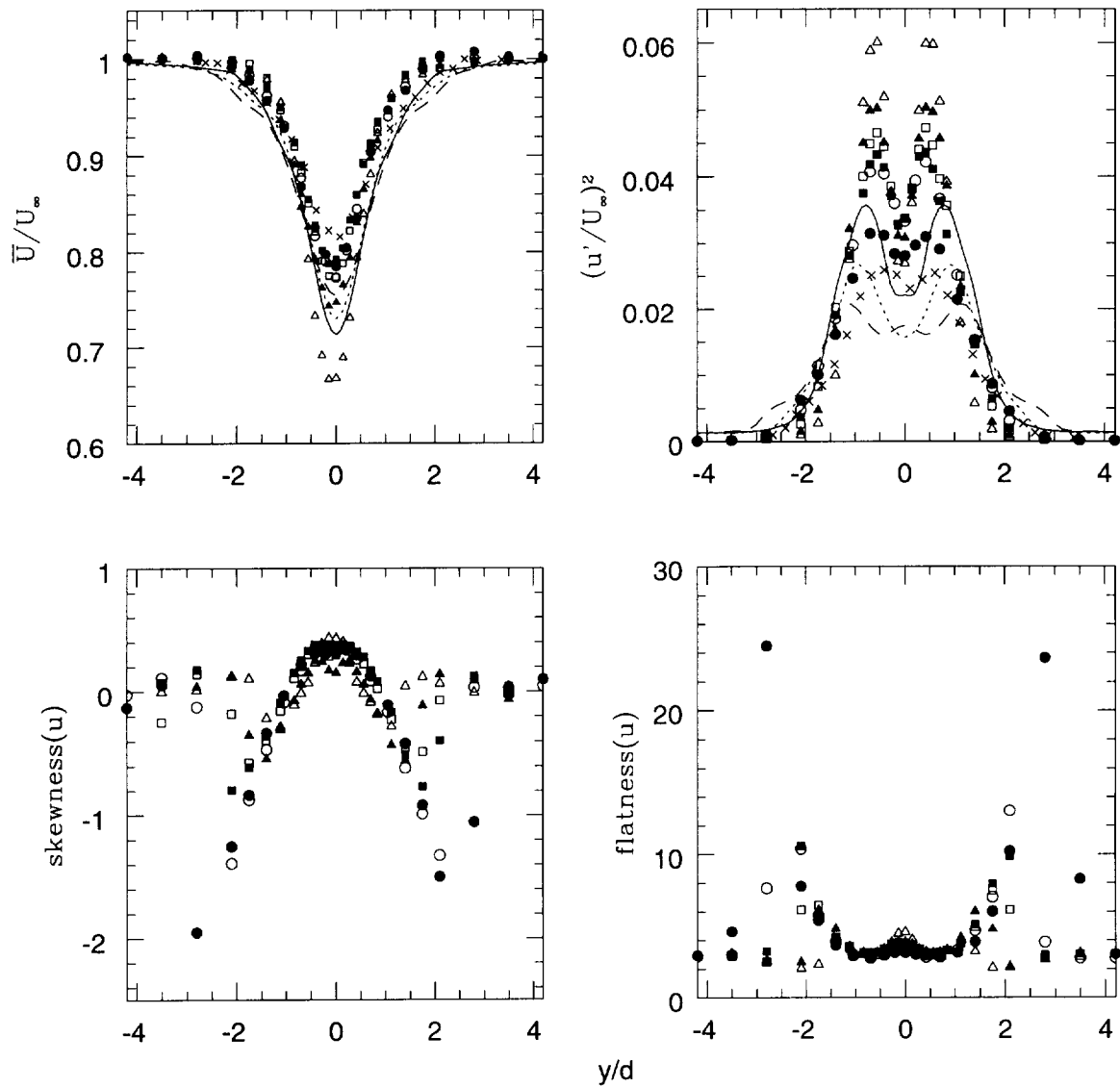| Distances from the cylinder, x/d	Present data	Beaudan et al.[1]	Zhou et al.[16]
3	△		
4	▲		
5	□	——	
6	■		
7	○	········	
10	●	- - -	×

Table 3: Symbols used in Figures 10 to 12.

Figure 10: Mean statistics of the u velocity component at various distances from the cylinder (see Table 3 for the symbols' definitions).

14

The u velocity component statistics exhibit the expected trend, ie. with increasing distance from the cylinder:

- the wake velocity deficit decreases,

- the peaks in the rms of the u-velocity component, u', decrease,

- the wake spreads as evidenced by the increased separation of the peaks of the skewness and flatness factors and, to a lesser extent, the velocity and rms profiles.

These profiles also show excellent symmetry about the wake centerline. As the skewness plots indicate, there are large positive velocity fluctuations near the center of the wake (positive skewness), and very much larger negative velocity fluctuations at the outer edges of the wake (negative skewness). In comparison to our experimental values, the LES overestimates the centerline velocity deficit, and underpredicts the peak values in the rms. By examining the y/d locations of peaks in the wake, especially at $x/d = 10$, it can be deduced that the LES calculated a slightly wider wake than those of the present experiments as well as that of Zhou and Antonia[16]. This could possibly be due to the difference in the level of the freestream turbulence intensity among the various studies, the effects of which certainly warrant further study. Without the freestream turbulence data from the two comparison data sets, such an analysis is not presently possible. Except at the wake's the outer edges and centerline, the velocity fluctuations are quite gaussian as indicated by flatness value of approximately 3.0 .

The v velocity component also exhibit the expected trends as described above for the u component. Although v values below ± 0.01 are beyond the resolution of the measurements, the anti-symmetry of the mean and skewness factors is clearly evident for all x/d locations of the present measurements. Similar to the mean u results, the LES predicted lower mean v values compared with those of the experiments. The $v - rms$, v', magnitude from the LES at $x/d = 5$ compares well with the experiments. The agreement between the LES and experiment for this v velocity component statistic is not as good for $x/d = 7$ and 10. At these locations, the LES peak values are about 16% lower compared to the experiments.

The Reynolds stress (uv) profiles are plotted on Fig. 12. The uv peaks increase in magnitude with decreasing distance from the cylinder. These peaks also move closer to the centerline due to the narrowing of the wake at x/d locations closer to the cylinder. While some discontinuities in the LES profiles, especially at $y/d = 0.5$ for the $x/d = 5$ location are observed, the uv magnitudes compare quite well with the experiments.
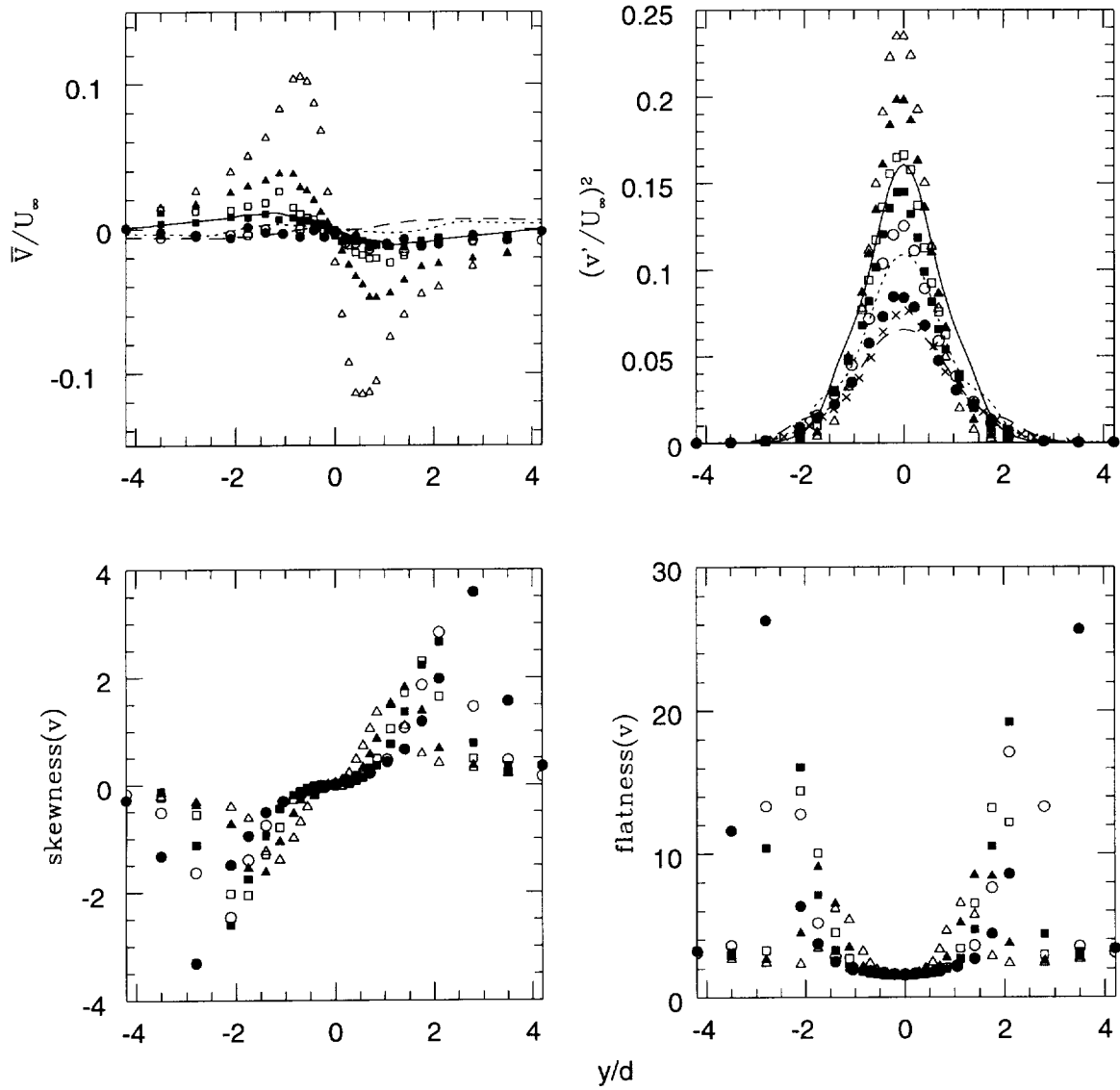
Figure 11: Mean statistics of the v velocity component at various x/d locations (see Table 3 for the symbols' definitions).
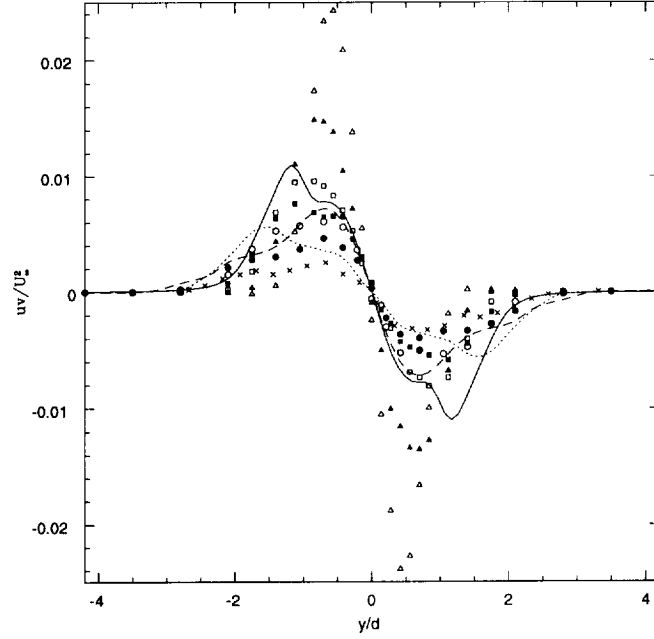
Figure 12: Reynolds stress (uv) profiles at various x/d locations (see Table 3 for the symbols' definitions).

6.2 Velocity Spectra

The spectra of the velocity components at $x/d=3,5,7$ and 10 , plotted with Kolmogorov scaling, are shown in Figs. 13 to 16. The -5/3 slope on these plots is represented by the dotted line and the vertical dashed line indicates the location of the low-pass filter cut-off frequency. At each x/d location, the spectra are plotted for the centerline and the approximate half-wake positions.

At the half-wake locations, the shedding frequency, $f_s = 64$, appear as the largest peaks on the spectral plots for both the u and v velocity component . The intensity of the u-spectral peaks at each axial station diminishes with decreasing distance from the centerline, where at $x/d = 7$ and 10 these centerline $(y/d = 0)$ spectra peaks are indistinguishable from the background levels. These centerline u-spectral peaks are weakest compared to the others. While the first and second harmonics of the shedding frequency also appear clearly in the spectra plots at the half-wake locations, the centerline plots of the v-spectra shows only the presence of the second harmonic. These results are consistent with those of Nguyen[14], who also indicated that the observed trend of the peaks can be predicted from linear stability theory.
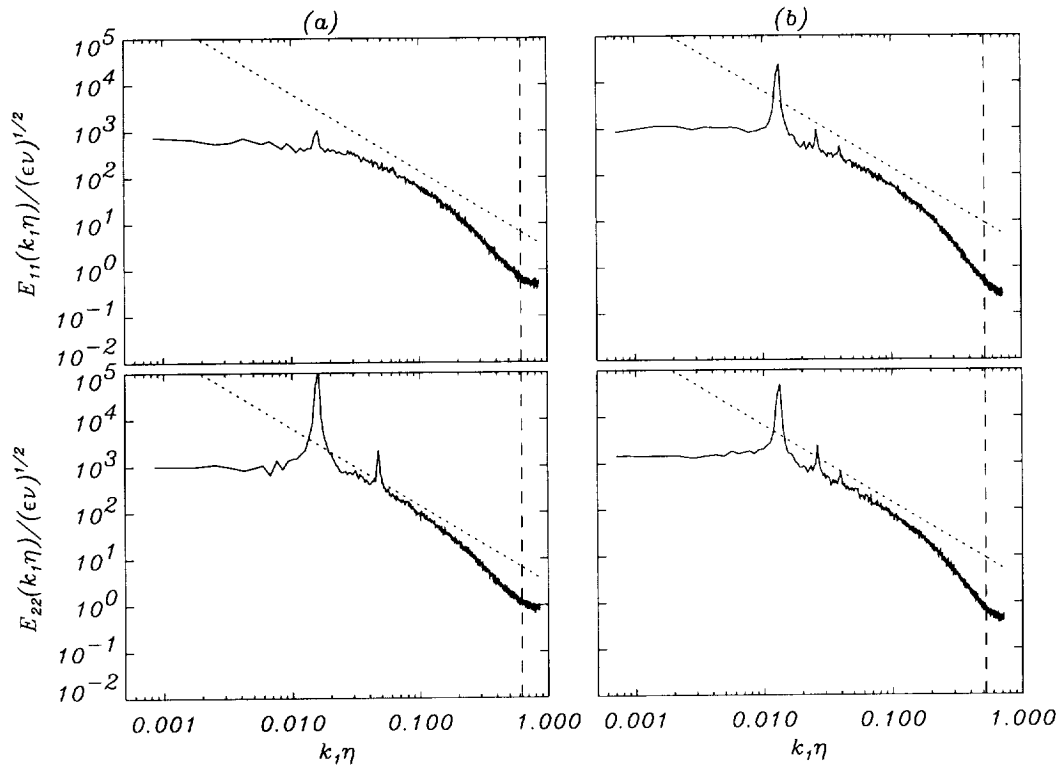
17

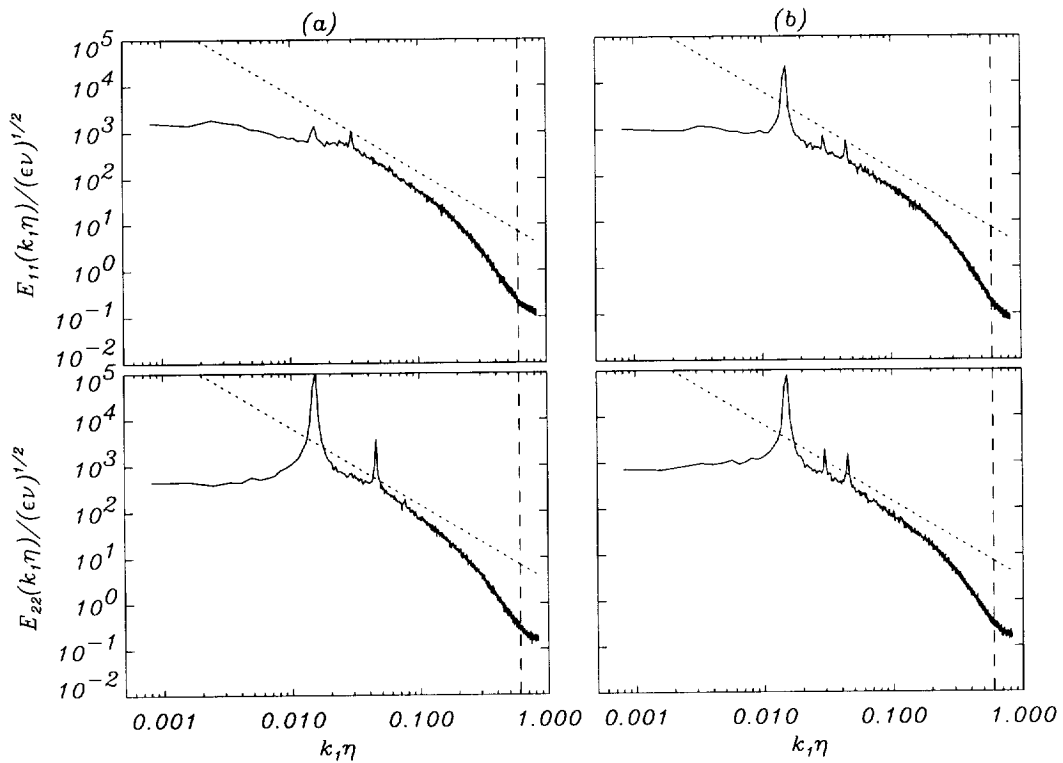Figure 13: Spectra at $x/d = 3$: (a) $y/d = 0$, (b) $y/d = 0.56$.

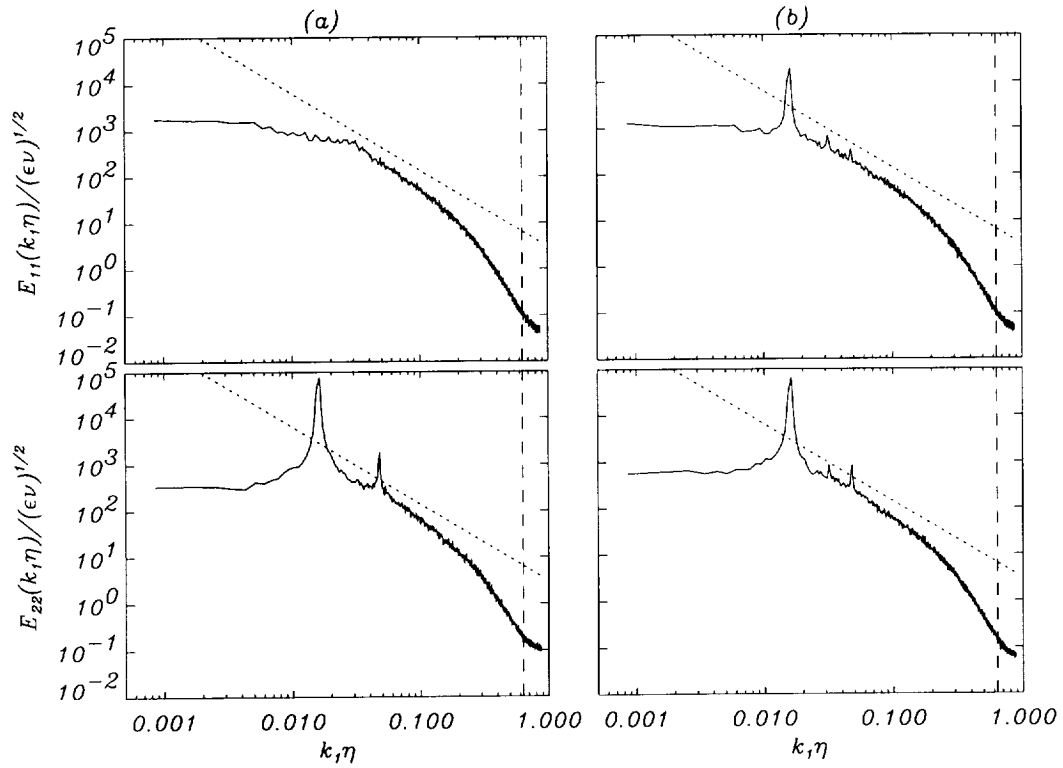Figure 14: Spectra at $x/d = 5$: (a) $y/d = 0$, (b) $y/d = 0.42$.

18

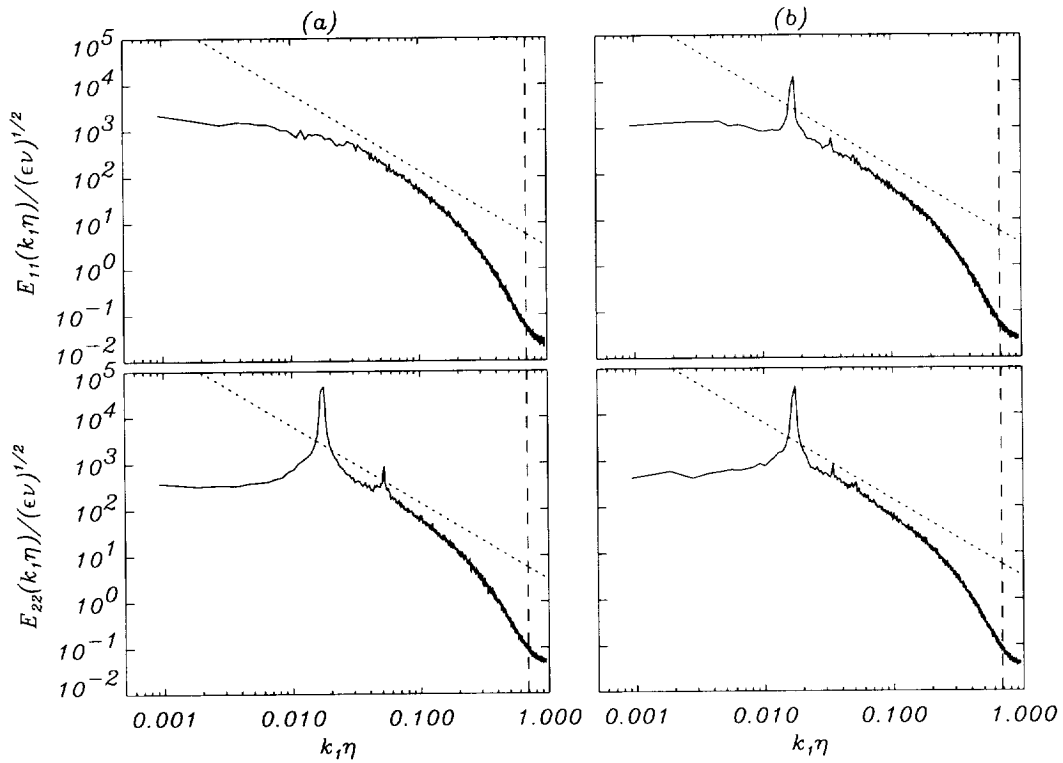Figure 15: Spectra at $x/d = 7$: (a) $y/d = 0$, (b) $y/d = 0.42$.

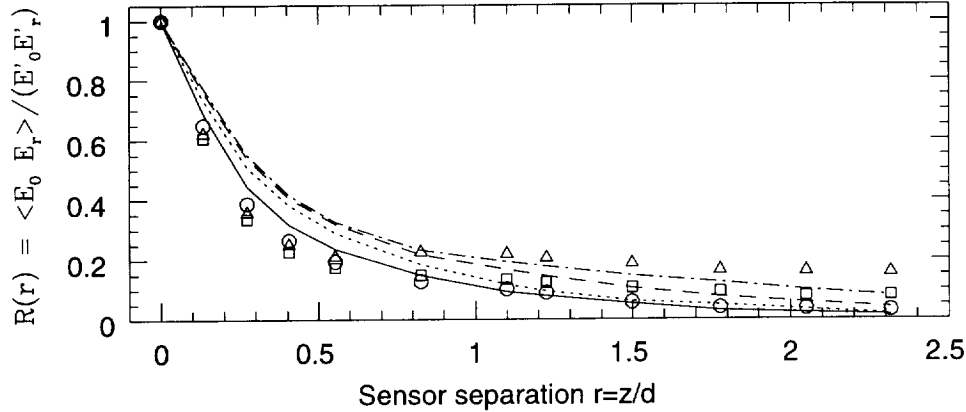Figure 16: Spectra at $x/d = 10$: (a) $y/d = 0$, (b) $y/d = 0.7$.

19

Figure 17: Spanwise cross-correlation coefficients at selected downstream locations from the cylinder, x/d: △ 2.5, □ 3, o 3.5, —— 4, --- 5, ———— 7,—·—· 10.

6.3 Spanwise Correlation Length Measurements

Simultaneous multi-point measurements in the spanwise direction were performed at $x/d = 2.5$, 3, 3.5 4, 5, 7, and 10 using a multi-sensor rake. Figure 17 shows the spatial correlation coefficient plotted against the normalized sensor separation. The data trend in this plot indicates that the spanwise correlation length decreases from $x/d = 2.5$ to $x/d = 4$. This is expected, because with increasing sensor separation, the two signals should become less correlated. Not expected for this experiment is that the correlation coefficients do not decay to zero but instead they appear to asymptote to some small but significant values. Additionally, at $x/d > 4$, the spatial correlation lengths seem to increase again. There also appears to be a preferred cross-over point near $z/d = 0.5$ for the correlation coefficient curves of $x/d = 2.5$ to 4. Although one might attribute these observations to the 2-D nature of the flow, further investigation is required to obtain a better understanding of this finding.

7 4-wire probe measurements

The X-wire measurements presented earlier in this report assume and require that the flow is largely 2-D in nature. This set of 4-wire probe measurements was conducted to explore the extent of 3-dimensionality of the very near wake regions and thus, semi-quantitatively, to verify the accuracy of the X-wire measurements. These measurements were conducted at locations along the wake centerline where it was expected that 3-

20

D effects are most pronounced. Limited by the operational range of the 4-wire probe of $< 25^o$, the closest measurement position achieved without significant data loss was $x/d = 5$.

Figure 18 shows the joint-probability distribution functions (JPDF) of the pitch and yaw angles at $x/d = 5$, 7 and 10. At $x/d = 10$, the peaks of the contours are at approximately $\pm 15^o$. At $x/d = 5$, the position of the peaks in the contours increase to 20°. This trend is consistent with the increase in flow angle of attack as distance from the cylinder decreases.

While this plot shows that the data contains large pitch angles $> 20^0$, the contours appear to be contained within yaw angles of $\pm 10^o$. This demonstrates that the flow is fairly 2-D at these locations, thus verifying the use of X-wire for accurate measurements in this flowfield.

8 Closure

This study has determined that estimations of the streamwise velocity component in flowfields with large non-zero cross-stream components are not accurate. Similarly, X-wire measurements of the u and v velocity components in flows containing large w are also subject to the errors due to binormal cooling.

Using the LUT technique, and by calibrating the X-wire probe used here to include the range of expected angles of attack ($\pm 40^o$), accurate X-wire measurements of instantaneous u and v velocity components in the very near wake region of a circular cylinder has been accomplished. The approximate 2-dimensionality of the present flowfield was verified with 4-wire probe measurements, and to some extent the spanwise correlation measurements with the multi-sensor rake. Hence, binormal cooling errors in the present X-wire measurements are small.

References

[1] P. Beaudan and P. Moin. Numerical experiments on the flow past a circular cylinder at sub-critical Reynolds number. Technical Report TF-62, Stanford University, Thermal Sciences Div., Dept. of Mechanical Engineering, 1994.

[2] P. Bradshaw. *An Introduction to Turbulence and its Measurement*. Pergamon, NY, 1971.

[3] L.W.B. Browne, R.A. Antonia, and L.P. Chua. Calibration of X-probes for turbulent flow measurements. *Experiments in Fluids*, 7:201–208, 1989.
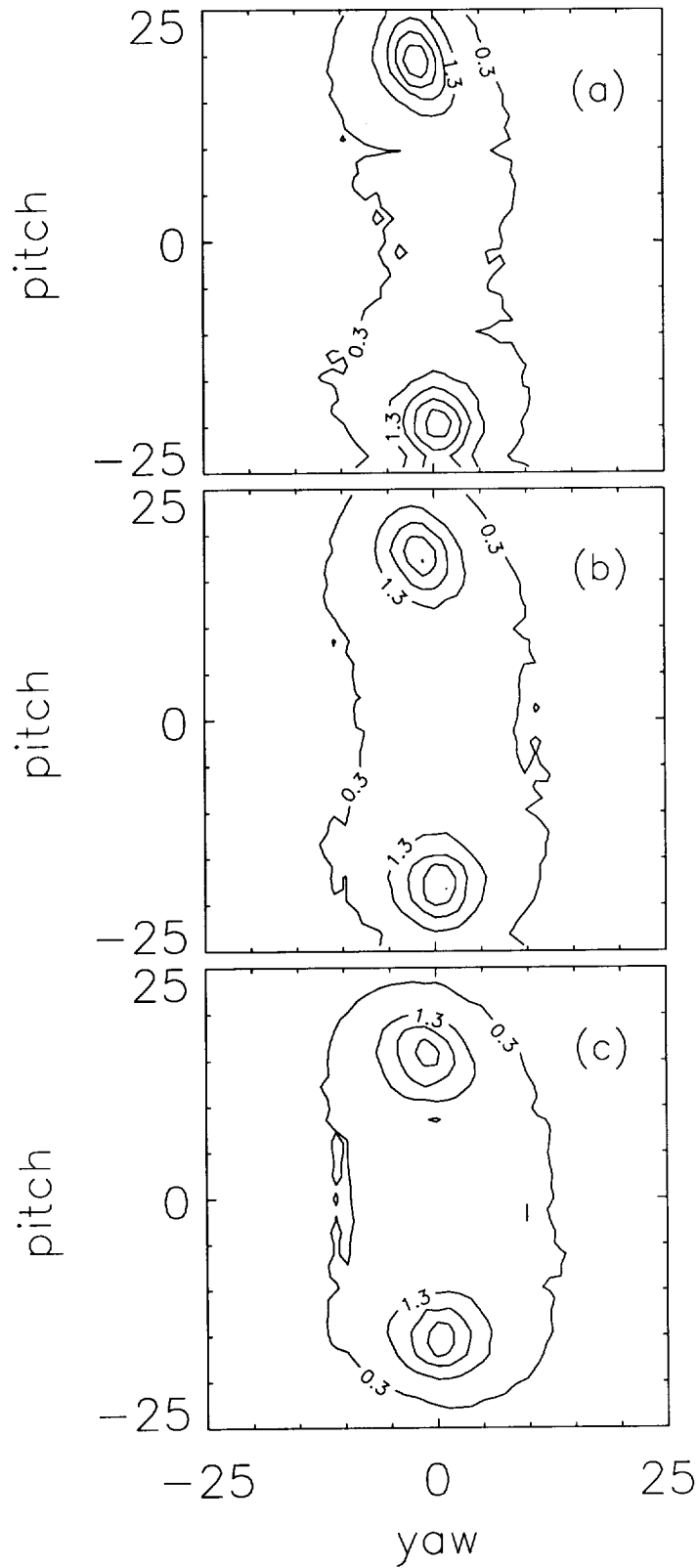
Figure 18: JPDF of the pitch and yaw angles along the wake centerline: (a) $x/d = 5$, (b) $x/d = 7$, (c) $x/d = 10$.

[4] H.H. Brunn. Hot-wire data corrections in low and high turbulence intensity flows. *J. Phys. E: Sci. Instrum*, 5:812, 1972.

[5] G. Buresti and N. R. Di Cocco. Hot-wire measurement procedures and their appraisal through a simulation technique. *J. Phys. E: Sci. Instrum.*, 20:87–99, 1987.

[6] F.H. Champagne, C.A. Sleicher, and O.H. Whermann. Turbulence measurements with inclined hot-wires. part 1 & 2. *J. Fluid Mech.*, 28:153, 1967.

[7] C.A. Friehe and W.H. Schwarz. Deviations from the cosine law for yawed cylindrical anemometer sensors. *J. Appl. Mech*, pages 655–662, 1968.

[8] L. S. Gresko Jr. Characteristics of wall pressure and near-wall velocity in a flat plate turbulent boundary layer. Master's thesis, Massachusetts Institute of Technology, August 1988.

[9] F. D. Johnson and H. Eckelmann. A variable angle method of calibration for X-probes applied to wall bounded turbulent shear flow. *Experiments in Fluids*, 2:121–130, 1984.

[10] F.E. Jorgensen. Directional sensitivity of wire and fiber-film probes. In *DISA Information*, volume 11, page 31. DISA Electronics, 1971.

[11] L. M. Lueptow, K. S. Breuer, and J. H. Haritonidis. Computer aided calibration of X-probes using a look-up table. *Experiments in Fluids*, 6:115–118, 1988.

[12] B. Marasli, P. Nguyen, and J.M. Wallace. A calibration technique for multiple-sensor hot-wire probes and its application to vorticity measurements in the wake of a circular cylinder. *Experiments in Fluids*, 15(3):209, 1993.

[13] Udo R. Müller. On the accuracy of turbulence measurements with inclined hot wires. *J. Fluid Mech.*, 119:155–172, 1982.

[14] Phuc Ngoc Nguyen. *Simultaneous measurements of the velocity and vorticity fields in the turbulent near wake of a circular cylinder.* PhD thesis, University of Maryland, 1993.

[15] W.W. Willmarth and T.J. Bogar. Survey and new measurements of turbulent structure near the wall. *Phys. Fluids*, 20:S9–S21, 1977.

[16] Y. Zhou and R.A. Antonia. A study of turbulent vortices in the near wake of a cylinder. *J. Fluid Mech.*, 253:643–661, 1993.